Stopping, particle production and Υ suppression in heavy-ion collisions at the LHC

Georg Wolschin

Heidelberg University

Institut für Theoretische Physik

Philosophenweg 16

D-69120 Heidelberg

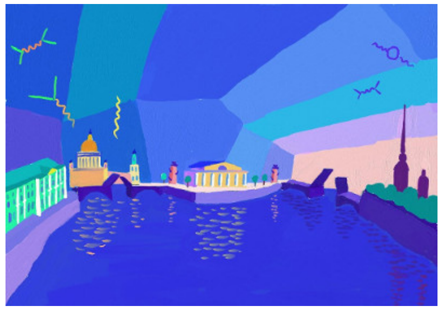

QFTHEP_2013

Topics

1. Introduction: Relativistic heavy ions @ LHC
2. Stopping in HI collisions
3. Particle production: Relativistic Diffusion Model (RDM)
4. Bottomium suppression in the Quark-Gluon Plasma (QGP)
5. Conclusion

1. Introduction

LHC detectors: Atlas, CMS, LHCb, ALICE

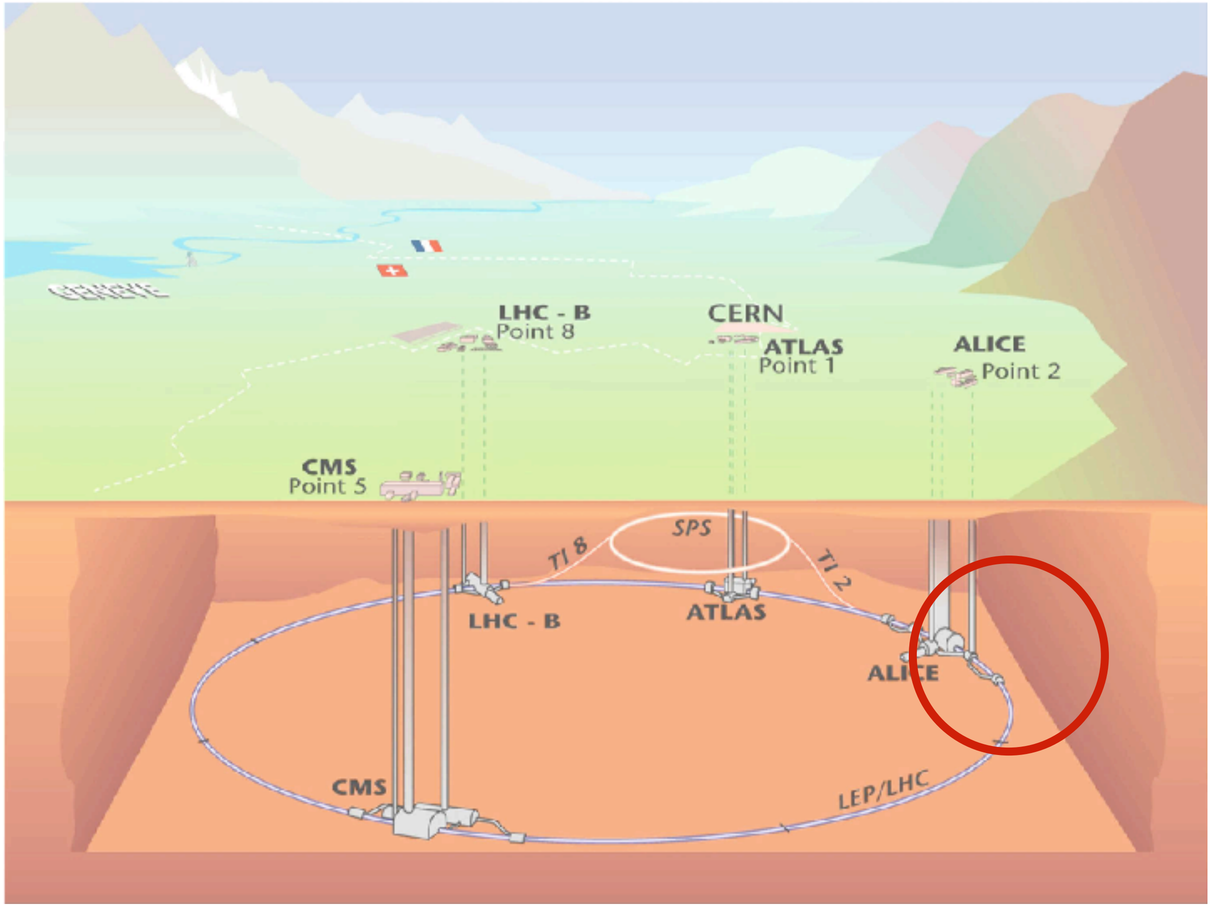

Pb - Pb at LHC:

max. 5.52 TeV/particle pair

1st lead beam Nov 6, 2010
@ 2.76 TeV

- PbPb @ 2.76 TeV 2011/12
- pPb @ 5.02 TeV 2012/13

- PbPb @ 5.52 TeV planned in 2015.

LHC Detectors

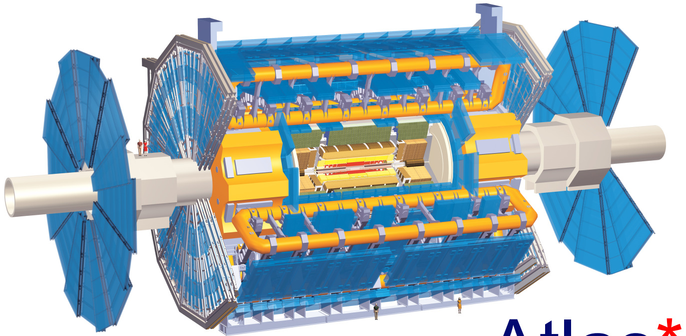

Atlas*

≈ 25 HI people

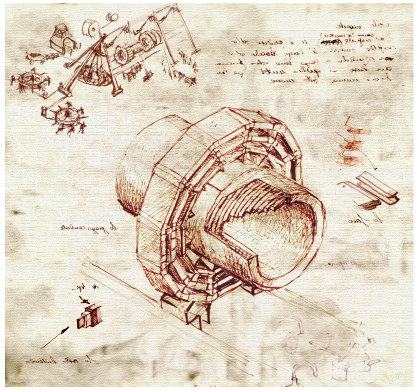

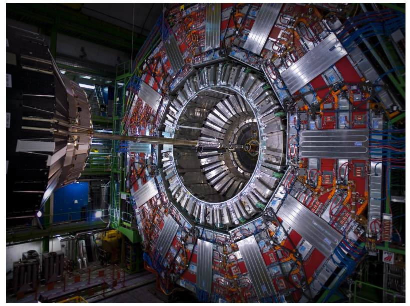

CMS*

da Vinci style

≈ 60 HI people

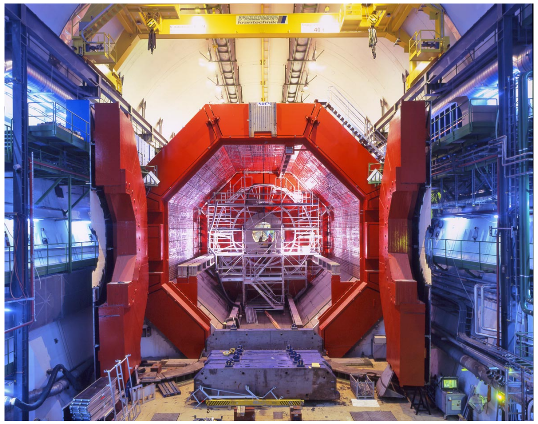

Alice*: L3 magnet

≈ 1,000 HI people

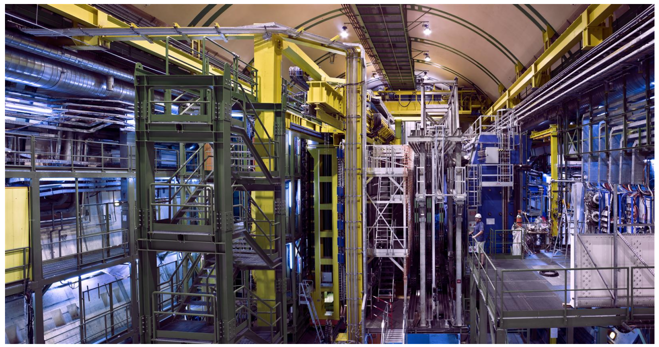

LHCb

p-Pb only

* heavy-ion capability

2. Stopping: Net protons/baryons and gluon saturation

Stopping occurs mainly through the interaction of valence quarks with gluons

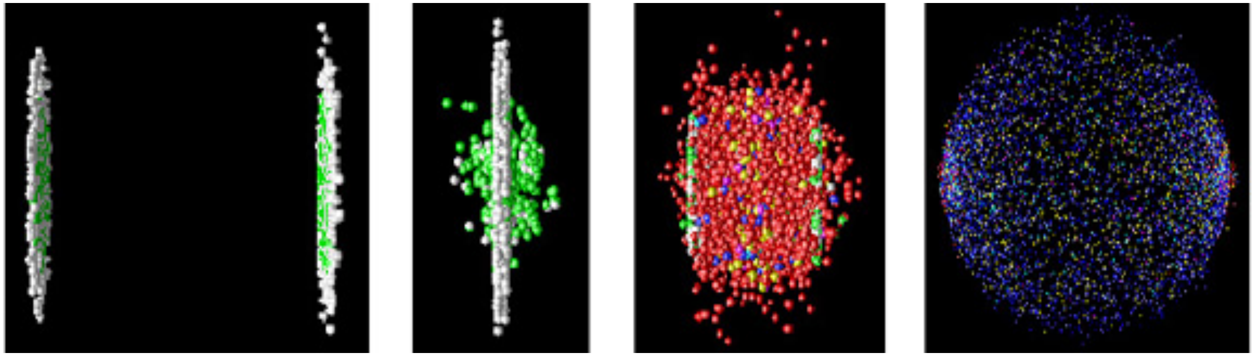

Artwork: UFRA

At RHIC (≤ 0.2 TeV) and LHC (≤ 5.52 TeV) energies, initially a state of very high gluon density is formed, which transforms into a strongly coupled quark-gluon plasma, and then hadronizes after $\approx 10^{-23}$ s into mesons and baryons.

Search for signatures of the QGP, and the initial Gluon Condensate in net-baryon (proton) distribution functions.

QCD

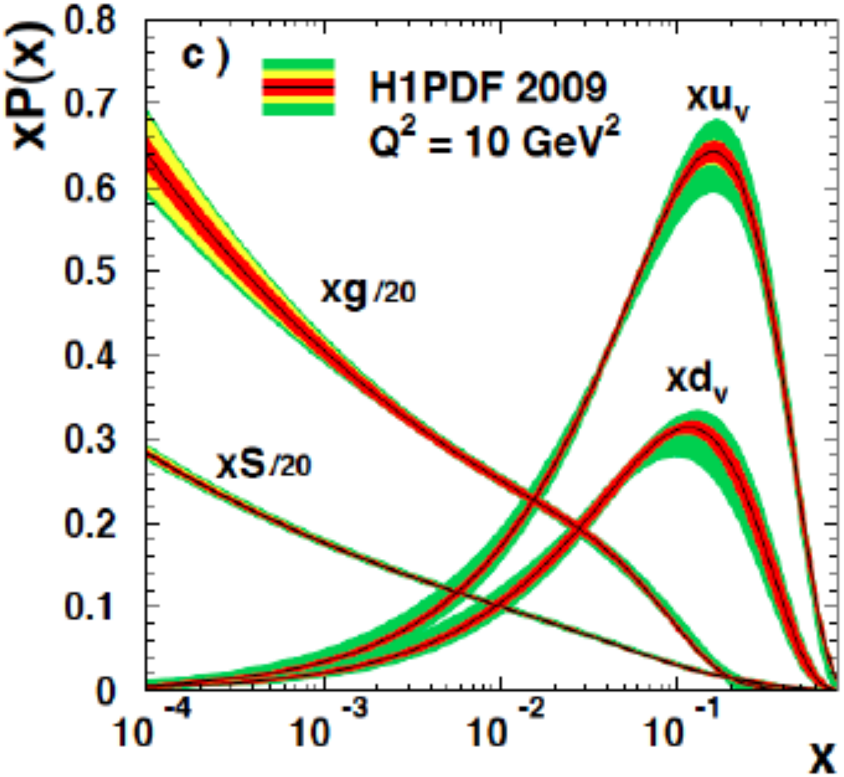

Structure functions (pdfs) from e + p deep inelastic scattering (DIS) at HERA (DESY)

- Gluon structure functions grow with increasing Q^2 and 1/x
- At small x and high energy, gluons dominate the dynamics.
- The gluon distribution should saturate at very small x. The saturation scale is $Q_s^2(x) \sim A^{1/3} x^{-\lambda}, \lambda \sim 0.3$

→ Saturation effects should be more pronounced in nuclei

Microscopic formulation of baryon transport for RHIC, LHC physics

- The net-baryon transport occurs through valence quarks:
- Fast valence quarks in one nucleus scatter in the other nucleus by exchanging soft gluons, and are redistributed in rapidity space.
- The valence quark parton distribution is well known at large x, which corresponds to the forward (and backward) rapidity region, and it can be used to access the small-x gluon distribution in the target.

Y. Mehtar-Tani and GW, Europhys. Lett. 94, 62003 (2011)
Phys. Lett. B688, 174 (2010)
Phys. Rev. C80, 054905 (2009)
Phys. Rev. Lett. 102,182301 (2009)

GW, Prog. Part. Nucl. Phys. 59, 374 (2007)
Phys. Rev. C 69, 024906 (2004)

The differential cross-section for valence quark production with rapidity y and transverse momentum p_T in a high-energy heavy-ion collision is

$$\frac{dN}{d^2p_T dy} = \frac{1}{(2\pi)^2}\frac{1}{p_T^2}\, x_1 q_v(x_1, Q_f)\, \varphi(x_2, p_T)$$

The contribution of the valence quarks in the forward moving nucleus to the rapidity distribution of hadrons is then (integration over p_T):

$$\frac{dN}{dy} = \frac{C}{(2\pi)^2}\int \frac{d^2p_T}{p_T^2}\, x_1 \underbrace{q_v}_{\text{Valence quarks}}(x_1, Q_f)\, \underbrace{\varphi}_{\text{Gluons}}(x_2, p_T)$$

Where the transverse momentum transfer is p_T,

the longitudinal momentum fraction carried by the valence quark is $x_1 = p_T/\sqrt{s}\exp(y)$

and the soft gluon in the target carries $x_2 = p_T/\sqrt{s}\exp(-y)$.

Starting from Eq. (4) in hep-ph/0211324 (A. Dumitru, L. Gerland, M. Stikman) and integrate it over k_t

$$\frac{d\sigma^{pA\to hX}}{dy d^2 b_t} = \frac{1}{2\pi}\int_0^{\sqrt{s}e^{-y}} \frac{dk_t}{k_t}\int_z^1 dx \frac{z}{x} f_{q/p}(x, Q_s)\ D_{h/q}(\frac{z}{x}, Q_s)\ \varphi(\frac{x}{z}k_t), \tag{1}$$

where $\varphi(k_t) = k_t^2 C(k_t)$. Recall that $z = \frac{k_t}{\sqrt{s}}\, e^y$. Performing the following change of variables

$$u = \frac{z}{x}, \tag{2}$$

$$\frac{x}{z}k_t = x\sqrt{s}e^{-y}, \tag{3}$$

Eq. (1) can be rewritten as

$$\begin{aligned}
\frac{d\sigma^{pA\to hX}}{dy d^2 b_t} &= \frac{1}{2\pi}\int_0^1 dz \int_z^1 \frac{dx}{x}\ D_{h/q}(\frac{z}{x}, Q_s)\ f_{q/p}(x, Q_s)\ \varphi(x\sqrt{s}e^{-y}), \\
&= \frac{1}{2\pi}\int_0^1 \frac{dx}{x}\left[\int_0^x dz\ D_{h/q}(\frac{z}{x}, Q_s)\right]\ f_{q/p}(x, Q_s)\ \varphi(x\sqrt{s}e^{-y}), \\
&= \frac{1}{2\pi}\int_0^1 \frac{dx}{x}\left[\int_0^1 du\ D_{h/q}(u, Q_s)\right]\ x f_{q/p}(x, Q_s)\ \varphi(x\sqrt{s}e^{-y}), \\
&\simeq \frac{C}{2\pi}\int_0^1 \frac{dx}{x}\ x f_{q/p}(x, Q_s)\ \varphi(x\sqrt{s}e^{-y}),
\end{aligned}$$

where $C \simeq \int_0^1 du\ D_{h/q}(u, Q_s)$, up to logarithms this is a constant.

Stopping in relativistic heavy-ion collisions

As in deep inelastic scattering, geometric scaling is expected:

The gluon distribution depends on x and p_T only through the scaling variable $p_T^2/Q_s^2(x)$ with the saturation scale

$$Q_s^2(x) = A^{1/3} Q_0^2 x^{-\lambda}$$

where $\lambda \approx 0.1 - 0.3$ (fit value in DIS at HERA is $\lambda \approx 0.3$ in agreement with next-to-leading order BFKL results of $\lambda = 0.288$).

Test this in comparison with SPS and RHIC data

Perform a change of variables

$$x \equiv x_1, \quad x_2 \equiv x\, e^{-2y}, \quad p_T^2 \equiv x^2 s\, e^{-2y}$$

then the rapidity distribution can be written as a function of a single scaling variable τ

$$\tau = \ln(s/Q_0^2) - \ln A^{1/3} - 2(1+\lambda)y$$

$$\frac{dN}{dy}(\tau) = \frac{C}{2\pi} \int_0^1 \frac{dx}{x}\, x q_v(x)\, \varphi(x^{2+\lambda} e^{\tau}).$$

For sufficiently large values of x, or the corresponding rapidity, the net-baryon rapidity distribution is a function of a **single** variable that relates the energy (s) dependence to the rapidity (y) and mass number (A) dependence.

There are 3 parameters: C, λ, Q_0.

Net-baryon rapidity distributions at SPS, RHIC, and LHC

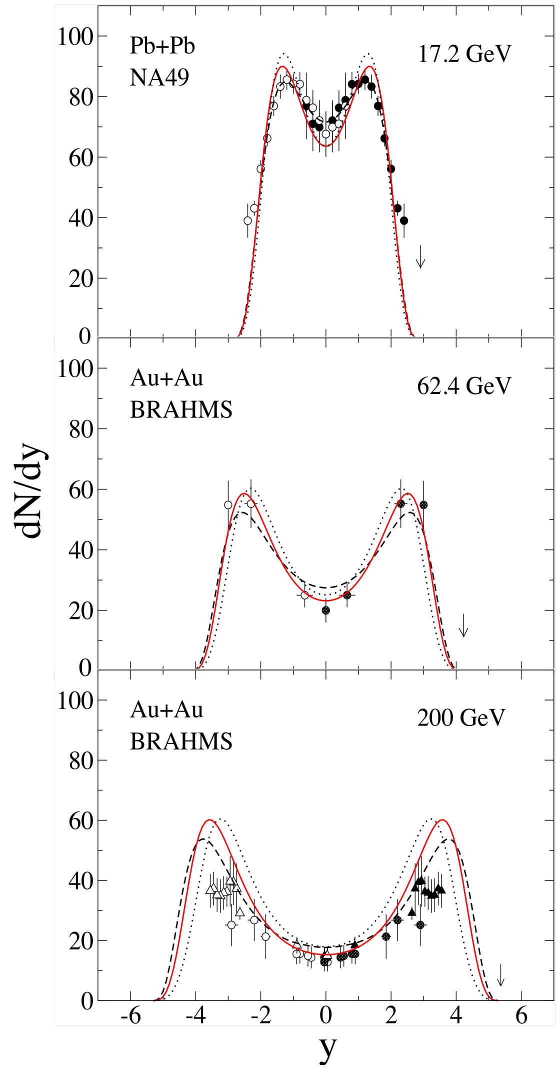

- Central (0-5%) Pb+Pb (SPS) and Au+Au (RHIC) Collisions

- Dashed black curves: Q_0^2 = 0.08 GeV^2 , λ=0
  Solid red curves: Q_0^2 = 0.07 GeV^2, λ=0.15
  Dotted black curves: Q_0^2 = 0.06 GeV^2, λ=0.3

- A larger gluon saturation scale produces more baryon stopping, as does a larger value of A.

- The saturation scale is $Q_s^2(x) = A^{1/3} Q_0^2 x^{-\lambda}$

Y. Mehtar-Tani and GW, Phys. Rev. Lett. 102,182301 (2009).

Net-baryon rapidity distributions at LHC: prediction

Particle identification region in ALICE

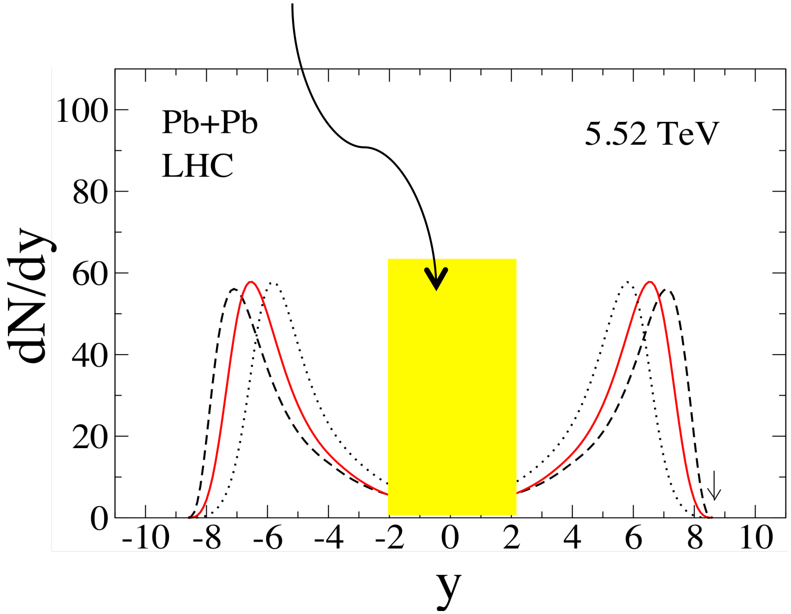

Y. Mehtar-Tani and GW
Phys. Rev. Lett. 102,182301 (2009)

- Central (0-5%) Pb+Pb collisions, $y_{beam} = 8.68$
- Dashed black curve: λ= 0
  Solid red curve: λ = 0.15
  Dotted black curve: λ= 0.3
- **A larger gluon saturation scale produces more baryon stopping; the fragmentation peak position is sensitive to λ**
- The midrapidity value of the net-baryon distribution is small, but finite: dN/dy (y = 0) ≈ 4. The **total yield** is normalized to the number of baryon participants, $N_B \approx 357$.

Measurements with particle identification will be confined to the yellow region for the next years

Net-proton rapidity distributions at RHIC and LHC

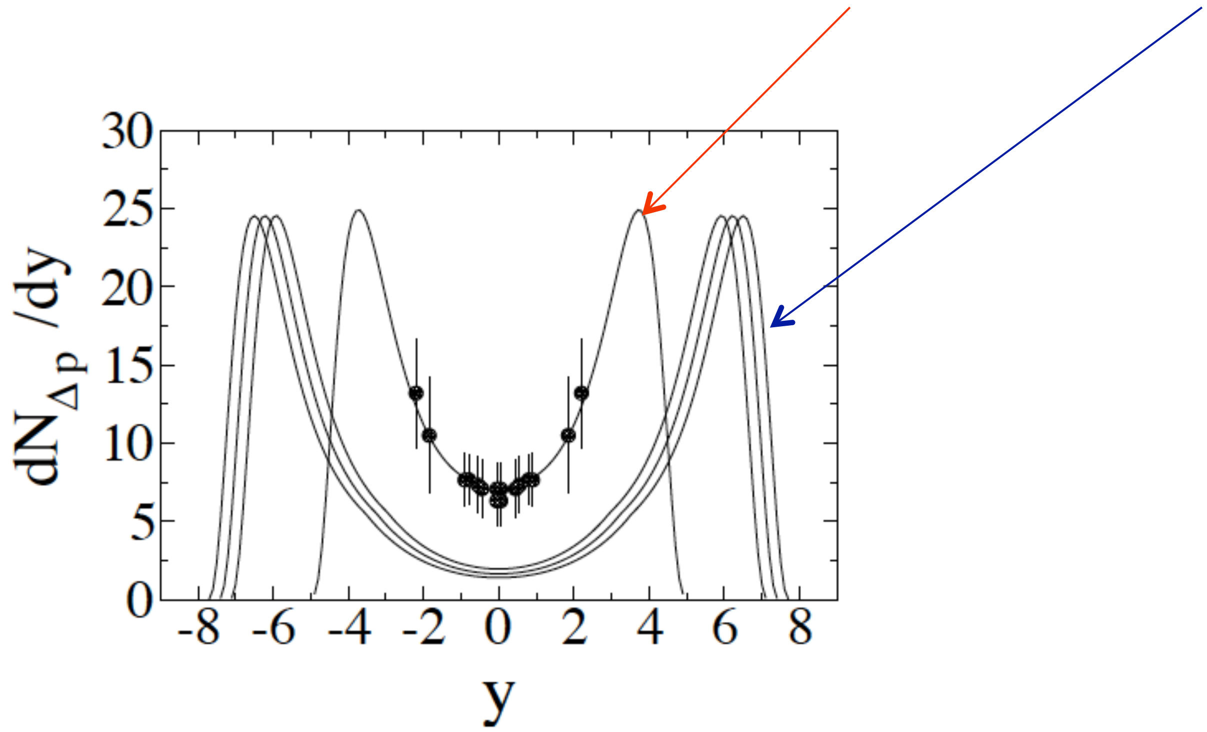

Figure 4: Calculated rapidity distributions of net protons in 0%–5% central Pb + Pb collisions at LHC energies of $\sqrt{s_{NN}} = 2.76, 3.94, 5.52$ TeV. Our result for central Au + Au collisions at RHIC energies of 0.2 TeV is compared with BRAHMS data [12] in a χ^2-minimization as in Fig. 1.

Y. Mehtar-Tani and G. Wolschin, Phys. Lett. B688, 174 (2010)

Mean rapidity loss: from AGS to LHC

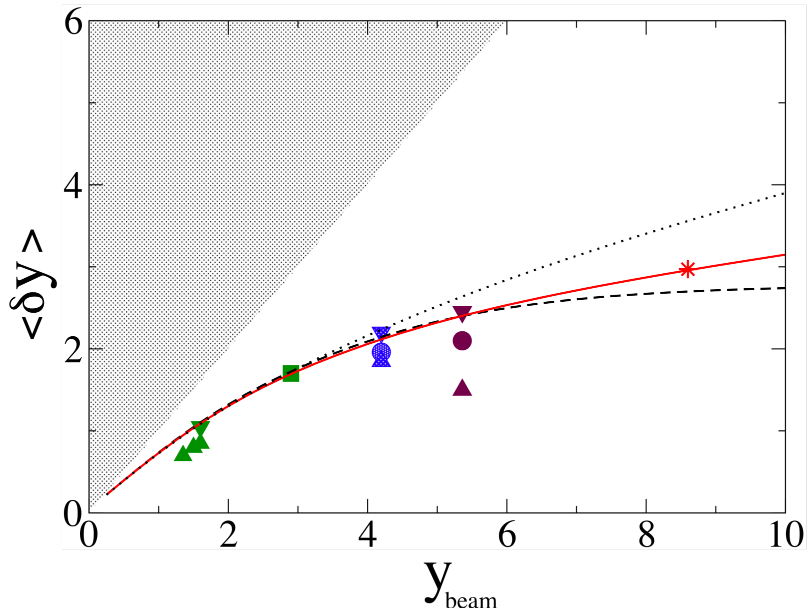

Dotted black curve: λ=0.3
Solid red curve: λ=0.2
Dashed black curve: λ=0
(no x-dependence: the mean rapidity loss reaches a limit at large beam rapidities)

red star: theoretical prediction for LHC

Hence, the value of λ could be determined in heavy-ion collisions at large energies (beam rapidities) above RHIC energies from the mean rapidity loss, or the peak position.

62.4 GeV and 200 GeV RHIC data are from BRAHMS, Phys. Lett. B 677, 267 (2009). 17.3 GeV SPS data are from NA49, low-energy data from AGS.

Y. Mehtar-Tani and G.Wolschin, Phys. Rev. Lett. 102,182301 (2009).

Conclusion 2: Stopping

- In a QCD-based microscopic model, we have calculated the net-baryon transverse momentum and rapidity distributions for heavy systems at RHIC and LHC energies.

- LHC: The model allows (in principle) to determine the gluon saturation scale from data on the mean rapidity loss, or from the position of the fragmentation peaks of net-baryon distributions in future forward-physics experiments.

- Midrapidity Pb + Pb results at LHC energies have been obtained in the microscopic model, and will be compared to net-proton (and net-kaon) data once available.

3. Particle production: Relativistic Diffusion Model (RDM)

$$\frac{\partial}{\partial t}R(y,t) = -\frac{\partial}{\partial y}\Big[J(y)R(y,t)\Big] + D_y\frac{\partial^2}{\partial y^2}[R(y,t)]^{2-q}$$

R (y,t) Rapidity distribution function. The standard linear Fokker-Planck equation corresponds to q = 1, and a linear drift function. For the three components k = 1,2,3 of the rapidity distribution,

$$\frac{\partial}{\partial t}R_k(y,t) = -\frac{1}{\tau_y}\frac{\partial}{\partial y}\Big[(y_{eq}-y)\cdot R_k(y,t)\Big] + D_y^k\frac{\partial^2}{\partial y^2}R_k(y,t)$$

Linear drift term with relaxation time τ_y Diffusion term, D_y=const.

Relaxation time and diffusion coefficient are related through a dissipation-fluctuation theorem. The broadening is enhanced due to collective expansion.

$$< y_{1,2}(t) >= y_{eq}[1-\exp(-t/\tau_y)] \mp y_{max}\exp\left(-t/\tau_y\right)$$ mean value

$$\sigma^2_{1,2,eq}(t) = D_y^{1,2,eq}\tau_y[1-\exp(-2t/\tau_y)]$$ variance

Linear Model: G. Wolschin, Eur. Phys. J. A5, 85 (1999); with 3 sources: Phys. Lett. B 569, 67 (2003); PLB 698, 411 (2011); M. Biyajima, M. Ide, M. Kaneyama, T. Mizoguchi, and N. Suzuki, Prog. Theor. Phys. Suppl. 153, 344 (2004)

Diffusion of produced particles in pseudorapidity space

Pseudorapidity distributions of produced particles are obtained through the Jacobian transformation

$$\frac{dN}{d\eta} = \frac{dN}{dy}\frac{dy}{d\eta} = \frac{p}{E}\frac{dN}{dy} \simeq J(\eta, \langle m\rangle/\langle p_T\rangle)\frac{dN}{dy}$$

$$J(\eta, \langle m\rangle/\langle p_T\rangle) = \cosh(\eta)\cdot$$
$$[1 + (\langle m\rangle/\langle p_T\rangle)^2 + \sinh^2(\eta)]^{-1/2}.$$

GW, J.Phys. G40, 045104 (2013)
D. Roehrscheid, GW, Phys. Rev. C86, 024902 (2012)

with the rapidity distribution in the three-sources model

$$\frac{dN_{ch}(y, t=\tau_{int})}{dy} = N_{ch}^1 R_1(y, \tau_{int})$$
$$+ N_{ch}^2 R_2(y, \tau_{int}) + N_{ch}^{eq} R_{eq}(y, \tau_{int}).$$

and the rapidity

$$y = 0.5 \cdot \ln((E+p)/(E-p))$$

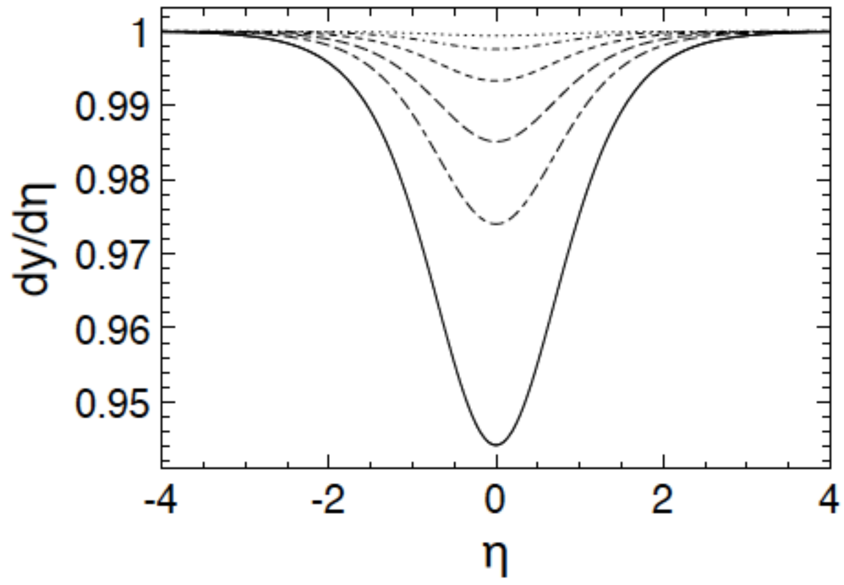

Figure 1: The Jacobian $dy/d\eta$ for $< m >= m_\pi$ and average transverse momenta (bottom to top) $< p_T >= 0.4, 0.6, 0.8, 1.2, 2$ and 4 GeV/c.

Comparing data with the RDM prediction

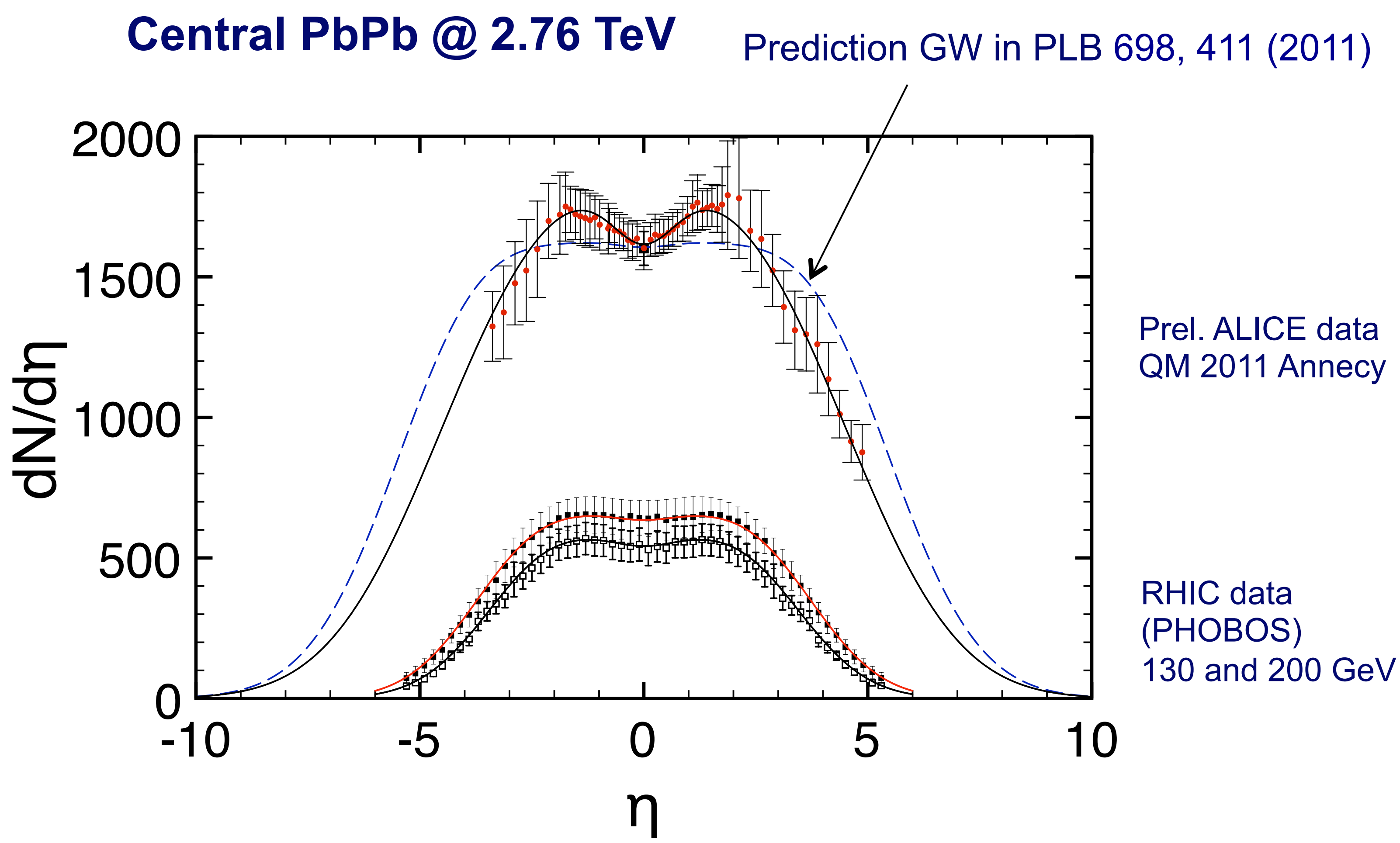

Comparison with RHIC and LHC data

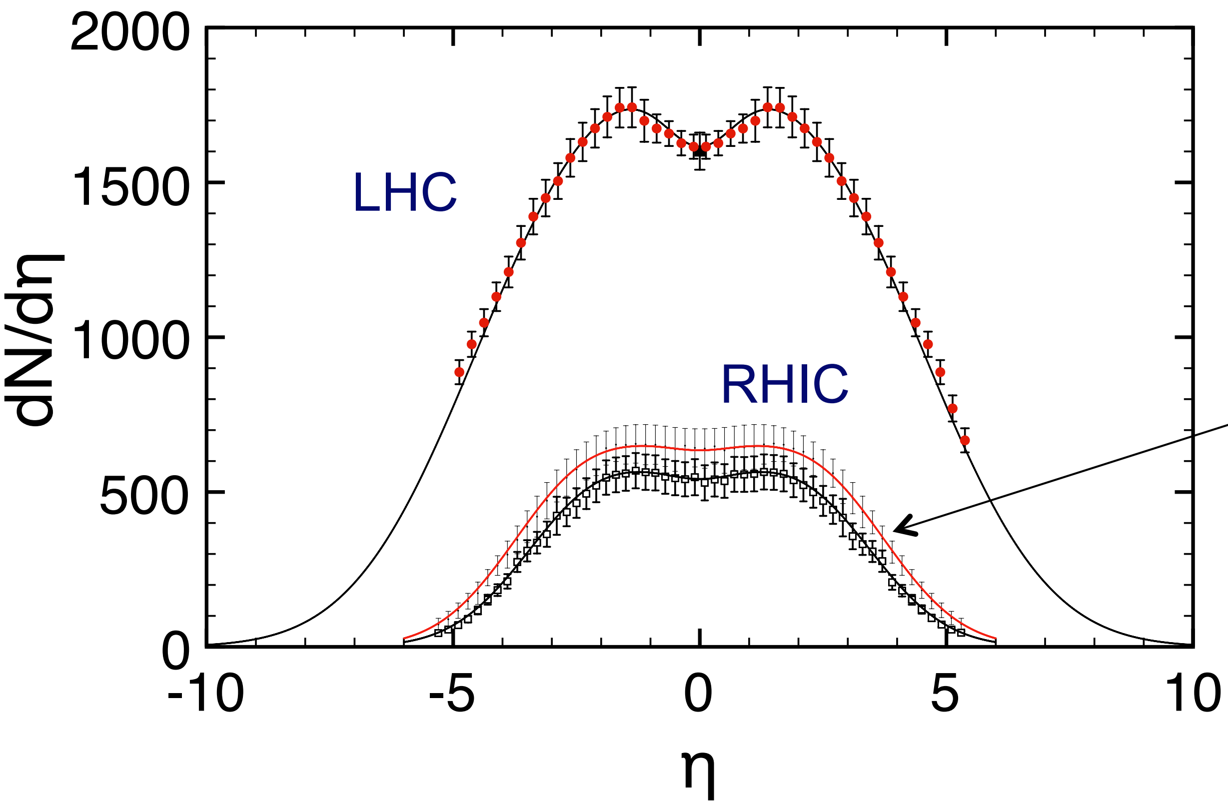

GW, J. Phys. G40, 045104 (2013)

LHC: PbPb@2.76 TeV 0-5% central collisions, RDM-result adjusted to ALICE dN/dη [prel. data K. Safarik et al, QM 2012 Washington]

RHIC: PHOBOS AuAu data 0-6% @ 0.13 and 0.2 TeV [3] with RDM-results (χ^2-minimization)

dN/dη (η≈0) = 1584 ± 4 (stat.) ± 76 (sys.) [1]
1601±60 [2]

[1] ALICE collab., PRL 105, 252301 (2010)

[2] ALICE collab., PRL 106, 032301 (2011)

[3] B.B. Back et al.,PHOBOS coll., PRL 87, 102303 (2001); PRL 91, 052303 (2003); PRC 83, 024913 (2011)

RDM χ^2 fits to prel. LHC/ALICE results for 2.76 TeV PbPb

GW, J. Phys. G40, 045104 (2013)

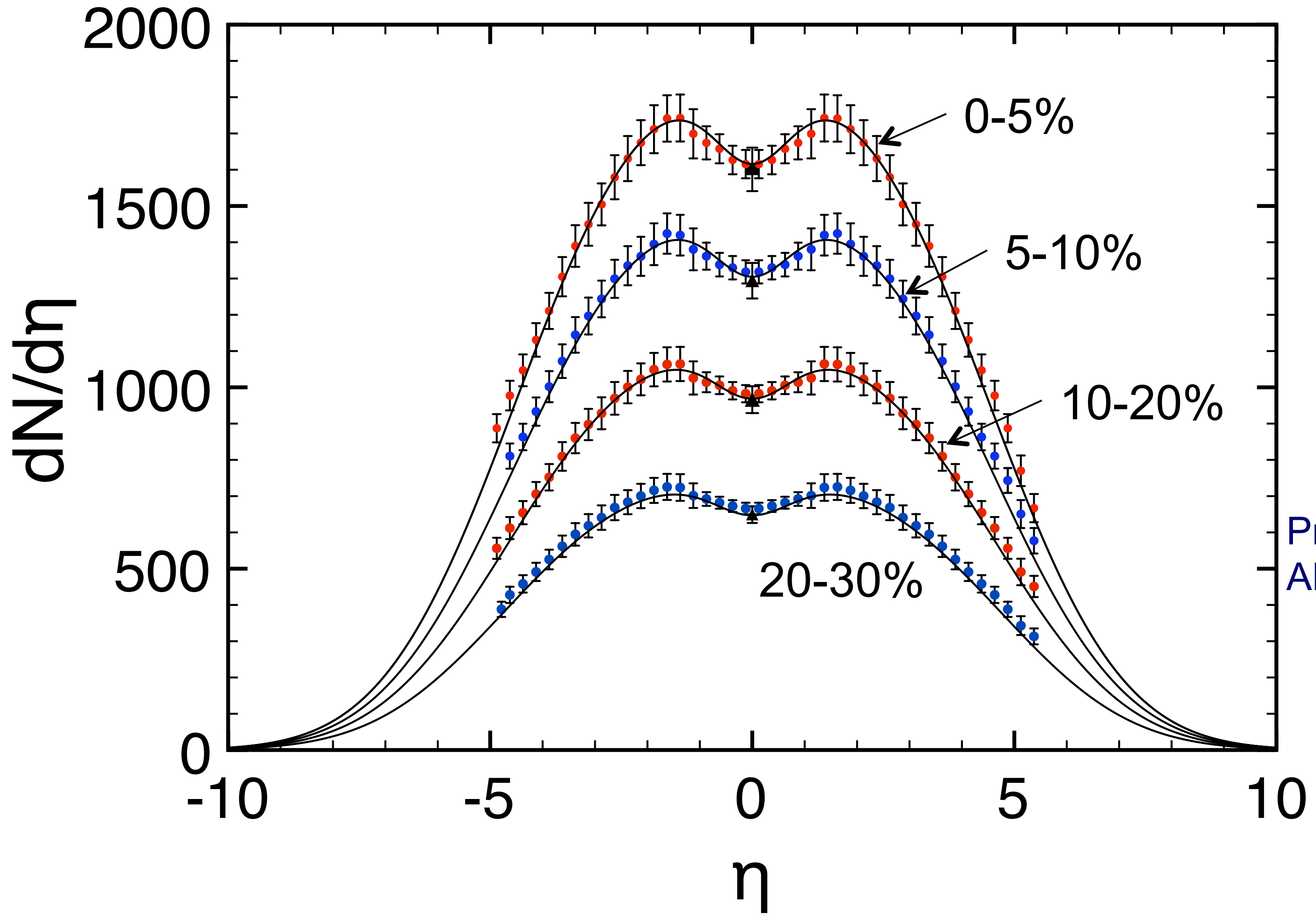

Prel.Data: K. Safarik et al.
ALICE Coll., QM2012

Parameters of the 3-sources RDM at RHIC and LHC energies

Table 1. Three-sources RDM-parameters τ_{int}/τ_y, $\Gamma_{1,2}, \Gamma_{gg}$, and N_{gg}. N_{ch}^{1+2} is the total charged-particle number in the fragmentation sources, N_{gg} the number of charged particles produced in the central source. Results for $< y_{1,2} >$ are calculated from y_{beam} and τ_{int}/τ_y. Values are shown for 0–5% PbPb at LHC energies of 2.76 and 5.52 TeV in the lower two lines, with results at 2.76 TeV from a χ^2-minimization with respect to the preliminary ALICE data [2], and using limited fragmentation as constraint. Corresponding parameters for 0–6% AuAu at RHIC energies are given for comparison in the upper four lines based on PHOBOS results [1]. Parameters at 5.52 TeV denoted by * are extrapolated. Experimental midrapidity values (last column) are from PHOBOS [1] for $|\eta| < 1$, 0-6% at RHIC energies and from ALICE [13] for $|\eta| < 0.5$, 0-5% at 2.76 TeV.

$\sqrt{s_{NN}}$ (TeV)	y_{beam}	τ_{int}/τ_y	$< y_{1,2} >$	$\Gamma_{1,2}$	Γ_{gg}	N_{ch}^{1+2}	N_{gg}	$\frac{dN}{d\eta}\|_{\eta\simeq 0}$
0.019	$\mp$3.04	0.97	$\mp$1.16	2.83	0	1704	-	314±23[1]
0.062	$\mp$4.20	0.89	$\mp$1.72	3.24	2.05	2793	210	463±34[1]
0.13	$\mp$4.93	0.89	$\mp$2.02	3.43	2.46	3826	572	579±23[1]
0.20	$\mp$5.36	0.82	$\mp$2.40	3.48	3.28	3933	1382	655±49 [1]
2.76	$\mp$7.99	0.87	$\mp$3.34	4.99	6.24	7624	9703	1601±60 [13]
5.52	$\mp$8.68	0.85*	$\mp$3.70	5.16*	7.21*	8889*	13903*	1940*

3 sources, and prediction for 5.52 TeV PbPb

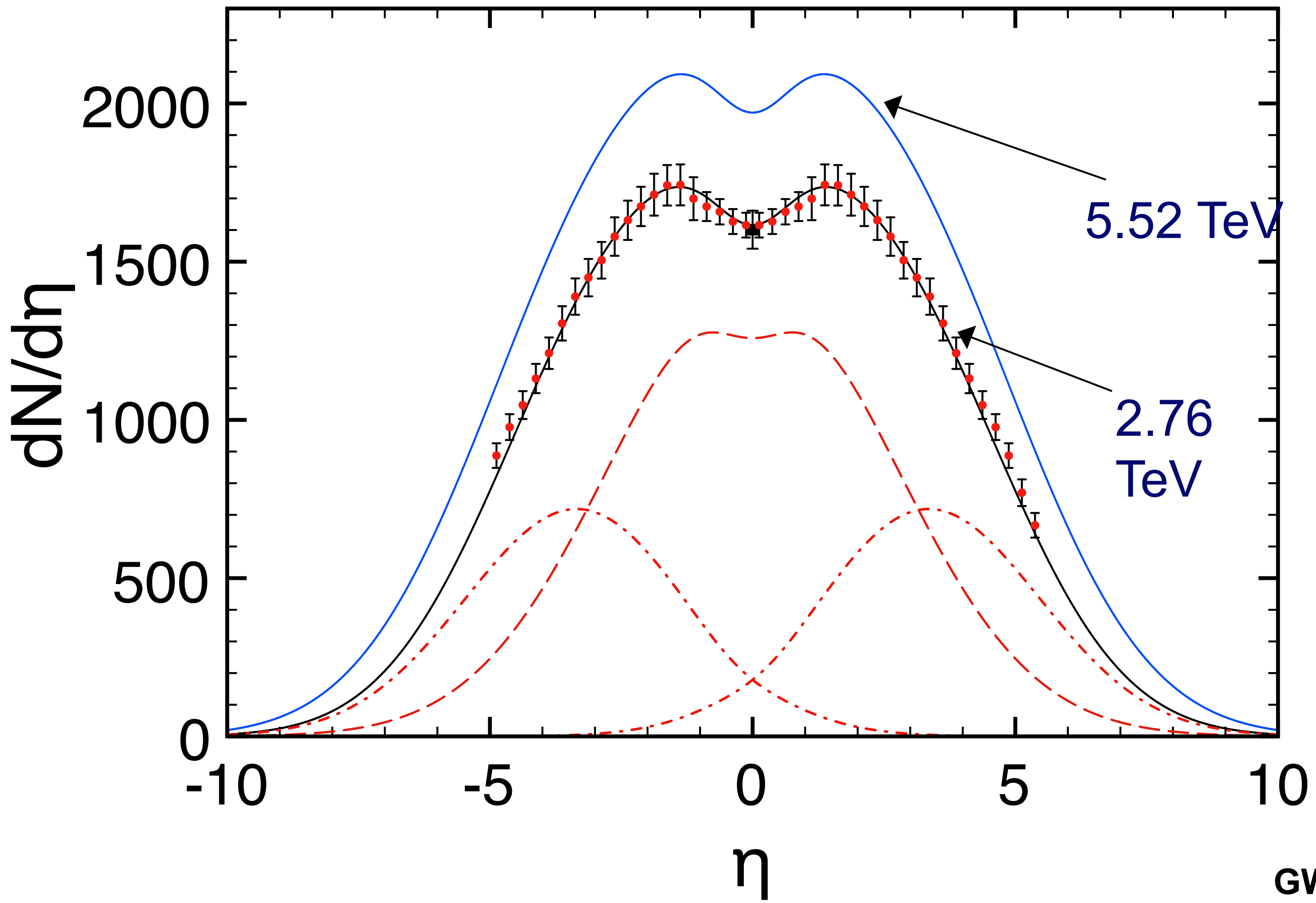

Centrality 0-5%

GW, J. Phys. G40, 045104 (2013)

LHC: Small fragmentation-source contributions at midrapidity

Charged hadrons

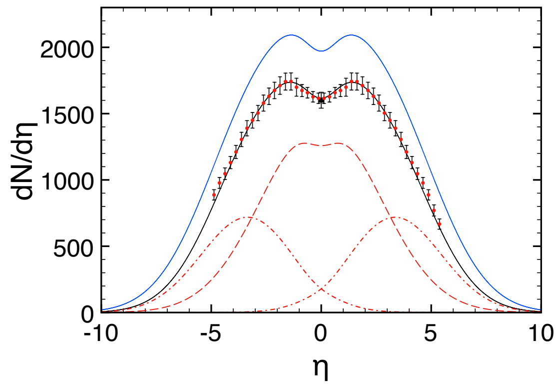

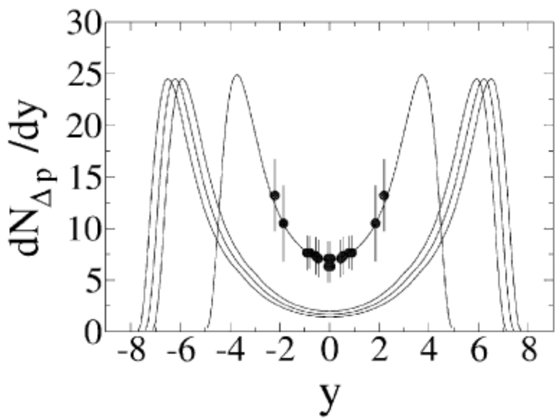

Net protons

YMT&GW, Phys. Lett. B688, 174 (2010);
GW, Phys. Lett. B 698, 411 (2011)

PbPb @ 2.76 TeV:

The smallness of the fragmentation sources at midrapidity is in qualitative agreement with results from our QCD-based microscopic model

Y. Mehtar-Tani and GW, Phys. Rev. Lett. 102,182301 (2009); PRC C80, 054905 (2009)

for net-baryon distributions, which indicates a midrapidity net-baryon yield dN/dy(y=0) ≈ 4, corresponding to 12 valence quarks, as cp. to 1248 valence quarks in the system (the net-baryon distribution has no gluon-gluon source)

Content of the sources as function of energy

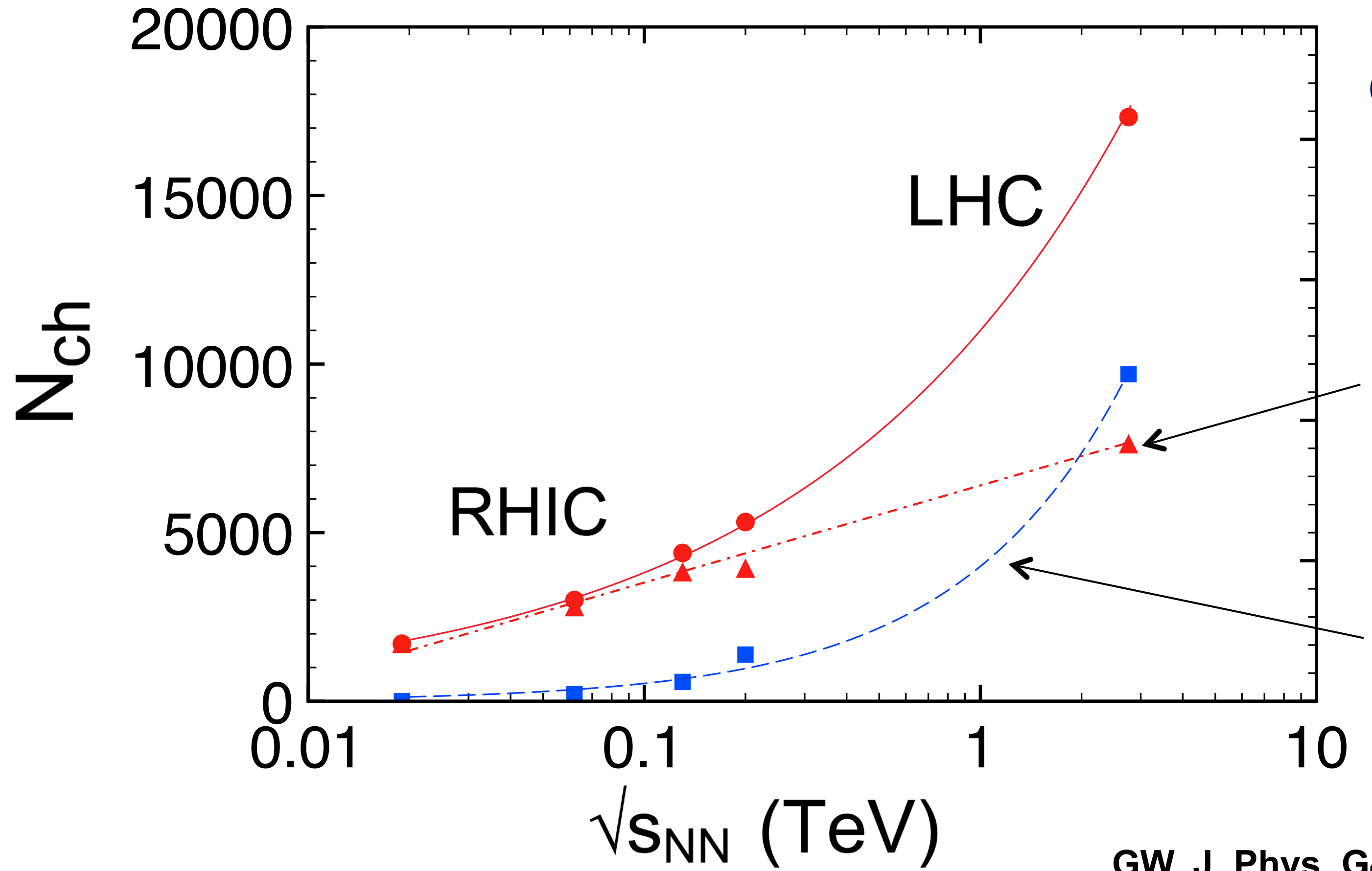

Centrality 0-5%

(RHIC 0-6%)

Fragmentation sources
$\sim \log(s_{NN}/s_0)$

Central source
$\sim s_{NN}^{0.44}$

GW, J. Phys. G40, 045104 (2013)

Charged-hadron distributions in pp: 3-sources relativistic diffusion model (RDM)

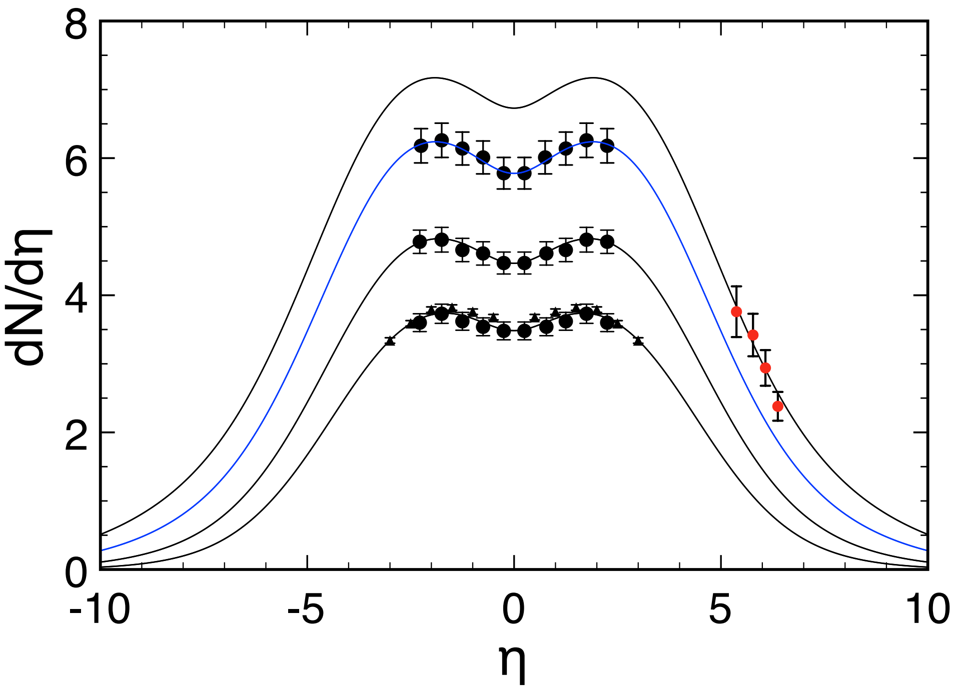

14 TeV pp

7 TeV

2.36 TeV

0.9 TeV (LHC injection energy / UA5)

Data: CMS collab., V. Khachatryan et al., J. High Energy Phys. 02, 041 (2010); Phys. Rev. Lett. 105, 022002 (2010); UA5 collab., R. Ansorge et al., Z. Phys. C 83, 357 (1989); TOTEM collab., G. Antchev et al., EPL 98, 31002 (2012)

pp charged-hadron pseudorapidity data beyond η=2.5 needed

3-sources RDM calculation: see GW, EPL 95, 61001 (2011) [Europhys. Lett.]

3-sources model (RDM): Centrality dependence of the asymmetric dAu system @ 0.2 TeV

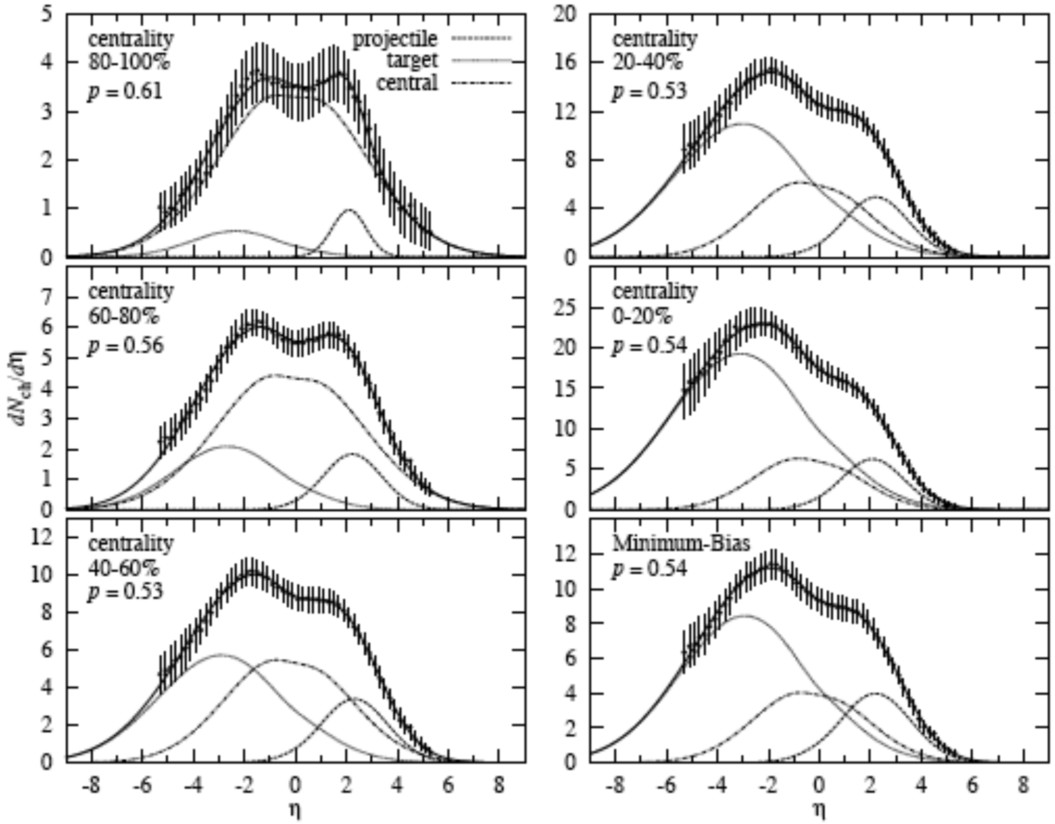

200 GeV dAu

PHOBOS data Phys. Rev. C72, 031901 (2005)

G. Wolschin, M.Biyajima,T.Mizoguchi, N.Suzuki, Annalen Phys. 15, 369 (2006)

Asymmetric systems are more sensitive to details of the nonequilibrium-statistical evolution than symmetric systems

3-sources model (RDM): Preliminary calc. for pPb @ 5.02 TeV

Min. bias 5.02 TeV pPb @ LHC

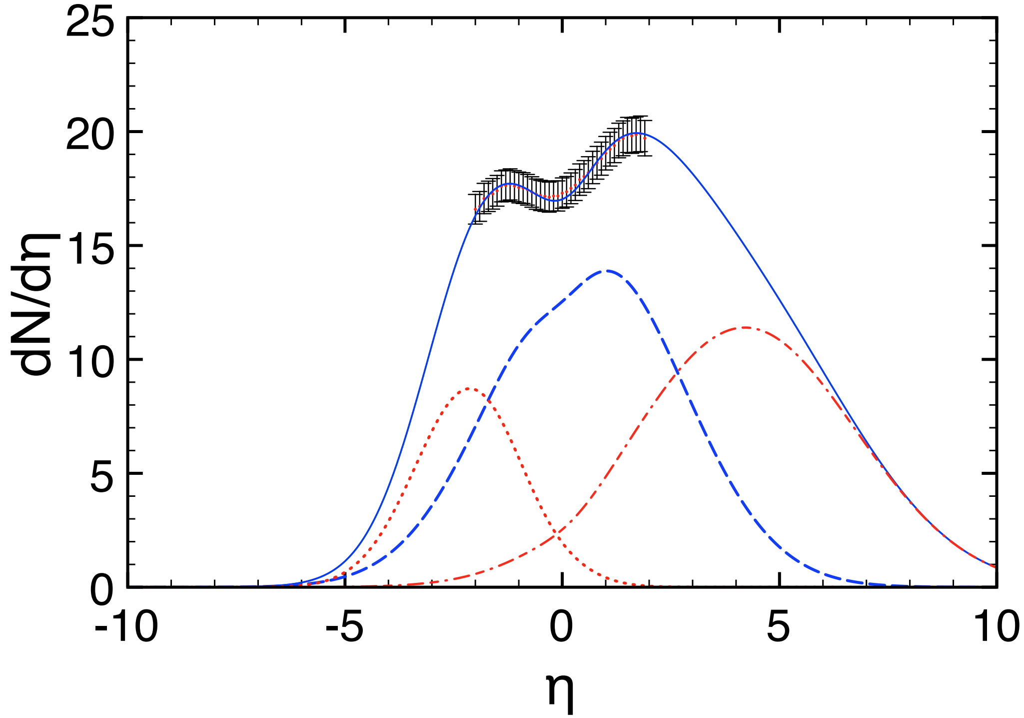

p_p= 4 TeV/c

$$\sqrt{s_{NN}} = \sqrt{\frac{Z_1 * Z_2}{(A_1 * A_2)}} * 2p_p = 5.02\mathrm{TeV}$$

$$y_{\mathrm{beam}}^{cm} = \mp \ln(\sqrt{s_{NN}}/m_0)$$
$$= \mp 8.586$$

Calculation: GW, J. Phys. G40, 045104 (2013)
Midrap. data: ALICE collab., PRL 110, 032301 (2013)

Conclusion 3: Particle production

- Charged-hadron production at RHIC and LHC energies has been described in a Relativistic Diffusion Model (RDM).

- Predictions of pseudorapidity distributions $dN/d\eta$ of produced charged hadrons in the 3-sources RDM at LHC energies rely on the extrapolation of the diffusion-model parameters with $\ln(\sqrt{s_{NN}})$

- In agreement with a QCD-based microscopic model, the contribution of the fragmentation sources from quark-gluon collisions at LHC energies is very small at midrapidity, but substantial at larger values of pseudorapidity η.

- Between RHIC and LHC energies, the midrapidity gluon-gluon source becomes more important than the fragmentation sources.

- **The centrality dependence** of the three sources has been investigated in direct comparison with the preliminary **ALICE data.**

4. Upsilon Suppression in PbPb @ LHC

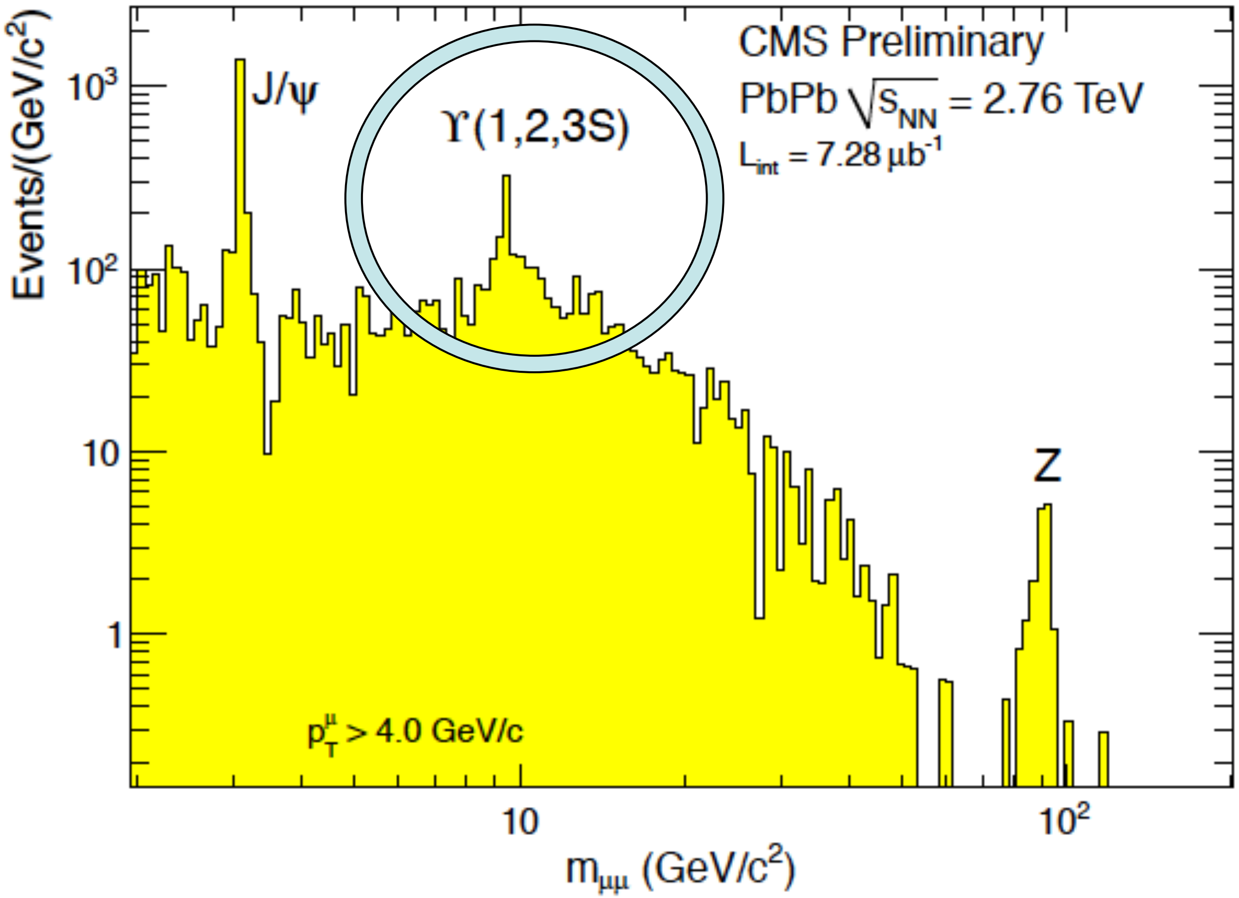

ϒ suppression as a sensitive probe for the QGP

- No significant effect of regeneration
- $m_b \approx 3m_c$ ⇨ cleaner theoretical treatment
- More stable than J/ψ

$E_B(\Upsilon_{1S}) \approx 1.10$ GeV
$E_B(J/\psi) \approx 0.64$ GeV

CMS Collab., CMS-PAS-HIN-10-006 (2011)

Υ(nS) states are suppressed in PbPb @ LHC:

CMS

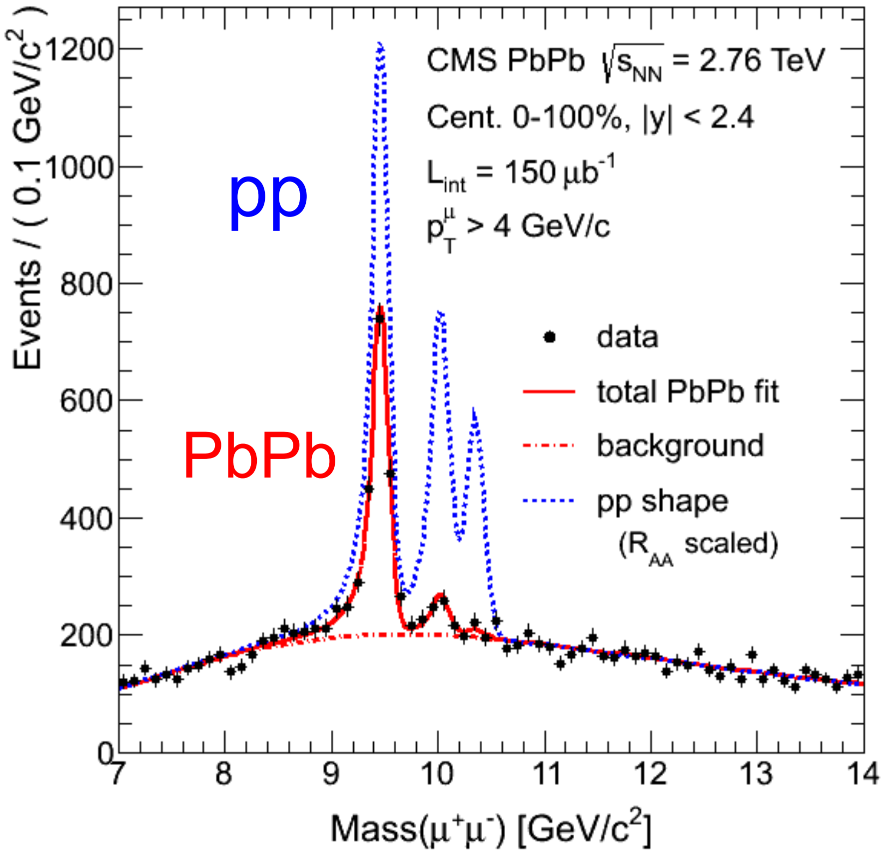

A clear QGP indicator

1. Υ(1S) ground state is suppressed in PbPb: R_{AA} (1S) = 0.56±0.08±0.07 in min. bias

2. Υ(2S, 3S) states are > 4 times stronger suppressed in PbPb than Υ(1S)

R_{AA}(Υ(2S)) = 0.12 ± 0.04 (stat.) ± 0.02 (syst.)

R_{AA}(Υ(3S)) = 0.03 ± 0.04 (stat.) ± 0.01 (syst.)

$$R_{AA} = \frac{N_{PbPb}(Q\bar{Q})}{N_{coll} N_{pp}(Q\bar{Q})}$$

CMS Collab., PRL 109, 222301 (2012)
[Plot from CMS database]

Screening, Gluodissociation and Collisional broadening of the Υ(nS) states

- Debye screening of all states involved: Static suppression
- Gluon-induced dissociation: dynamic suppression, in particular of the Υ(1S) ground state due to the large thermal gluon density
- The imaginary part of the potential (effect of collisions) contributes to the broadening of the Υ(nS) states: damping
- Feed-down from the excited Υ states to the ground state substantially modifies the populations: indirect suppression

F. Vaccaro, F. Nendzig and GW, Europhys.Lett. 102, 42001 (2013)
F. Nendzig and GW, Phys. Rev. C 87, 024911 (2013)
F. Brezinski and GW, Phys. Lett.B 70, 534 (2012)

Screening and damping treated in a nonrelativistic potential model

$$V(r,T) = \sigma r_D\left[1 - e^{-r/r_D}\right] - \frac{4\alpha_s^s}{3}\left[\frac{1}{r_D} + \frac{1}{r}e^{-r/r_D}\right]$$
$$-i\frac{4\alpha_s^s}{3}T\int_0^\infty dz\frac{2z}{(1+z^2)^2}\left[1 - \frac{\sin(rz/r_D)}{(rz/r_D)}\right]$$

Screened potential: r_D Debye radius, $\alpha_s^s \approx 0.37$ the strong coupling constant at the soft scale $\alpha_s^s = \alpha_s(m_b\alpha_s)$ accounting for short-range Coulomb exchange, $\sigma \approx 0.192$ the string tension (Jacobs et al.; Karsch et al.)

Imaginary part: Collisional damping (Laine et al. 2007, Beraudo et al. 2008)

$$r_D^{-1} = T\left[4\pi\alpha_s(2N_c + N_f)/6\right]^{1/2}$$ = m_D, Debye mass

Radial wave functions of Υ(nS) states

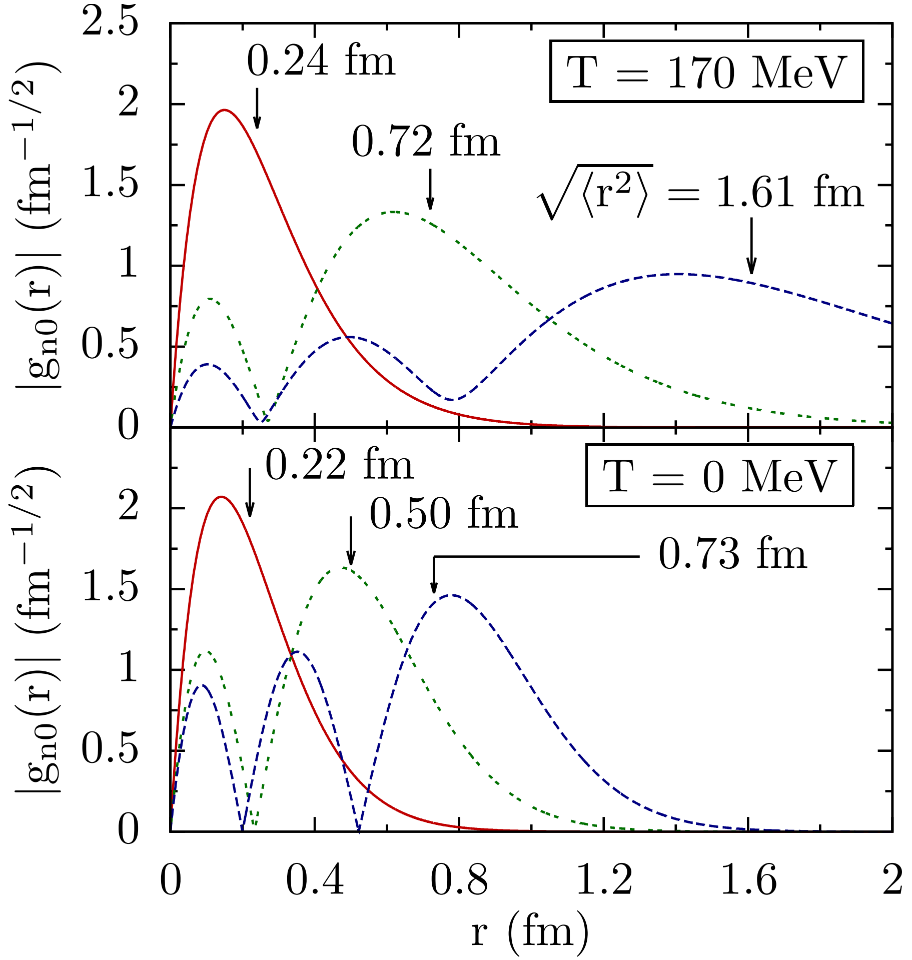

From the numerical solution of the Schoedinger equation with complex potential V(r)

$$\left[2m - \frac{\Delta}{2\mu} + V(r) - M\right]\psi(\vec{r}) = 0$$

Υ(1S) groundstate very stable against screening for T < 4.1 T_C

Figure 1: (color online) Radial wave functions of the Υ(1S), (2S), (3S) states (solid, dotted, dashed curves, respectively) calculated in the complex screened potential eq.(1) for temperatures $T = 0$ MeV (bottom) and 170 MeV (top) with effective coupling constant $\alpha_{eff} \simeq (4/3)\alpha_s^s = 0.49$, and string tension $\sigma = 0.192$ GeV^2. The rms radii $< r^2 >^{1/2}$ of the 2S and, in particular, 3S state strongly dependend on temperature T, whereas the ground state remains nearly unchanged.

From: F. Nendzig and G. Wolschin, arXiv:1207.6227 (Proc. HP2012)

Cross section for gludissociation

Born amplitude for the interaction of gluon clusters according to Bhanot&Peskin in dipole approximation / Operator product expansion

$$\mathcal{M} = \frac{1}{2}\frac{4\pi\alpha_s}{3}\frac{E^2}{3}\langle\psi|\vec{r}\left(\frac{1}{H_8+\epsilon-E}+\frac{1}{H_8+\epsilon+E}\right)\vec{r}\,|\psi\rangle$$

The cross section is obtained via the optical theorem from the forward scattering amplitude

$$\Im\mathcal{M}(t=0) = E\sigma$$

$$\sigma = \frac{1}{E}\cdot\frac{1}{2}\frac{4\pi\alpha_s}{3}\frac{E^2}{3}\langle\psi|\vec{r}\,\pi\delta\left(H_8+\epsilon-E\right)\vec{r}\,|\psi\rangle$$
$$= \frac{2\pi^2\alpha_s E}{9}\langle\psi|\vec{r}\,\delta\left(H_8+\epsilon-E\right)\vec{r}\,|\psi\rangle.$$

Gludissociation cross section in leading order, with coulombic wfct

Insert a complete set of eigenstates $|\chi_k\rangle$ of the adjoint repulsive (octet) Hamiltonian with eigenvalues k^2/m to consider also the string part of the potential:

$$\sigma = \frac{2\pi^2\alpha_s E}{9} \int_0^\infty dk\, \delta\left(k^2/m + \epsilon - E\right) \left| \int d^3x\, \vec{r}\, \psi(\vec{r}) \chi_k(\vec{r}) \right|^2$$

which yields an expression that can be extended to include the screened coulombic + string eigenfunctions

$$\sigma^{nS}_{diss}(E) = \frac{2\pi^2\alpha_s E}{9} \int_0^\infty dk\, \delta\left(\frac{k^2}{m_b} + \epsilon_n - E\right) |w^{nS}(k)|^2$$

$$w^{nS}(k) = \int_0^\infty dr\, r\, g^s_{n0}(r) g^a_{k1}(r)$$

for the Gluodissociation cross section.

Gludissociation cross section

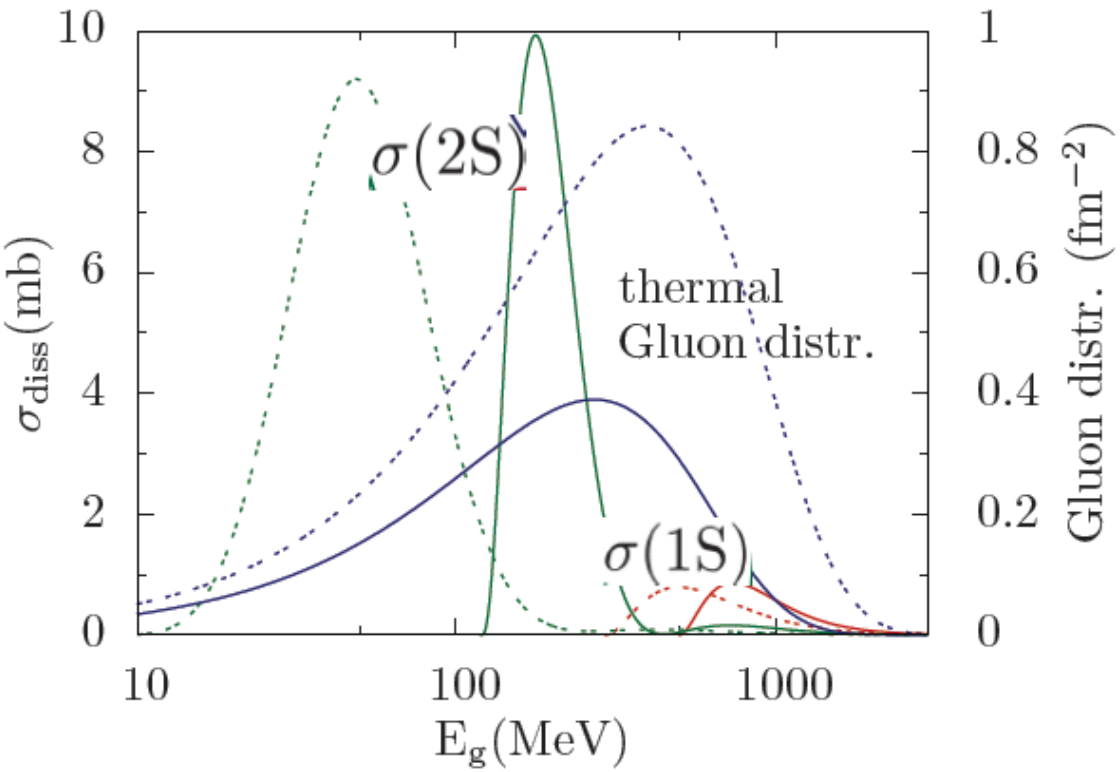

Figure 2: (color online) Gluodissociation cross sections $\sigma_{diss}(nS)$ in mb (lhs scale) of the $\Upsilon(1S)$ and $\Upsilon(2S)$ states calculated using the screened wave functions calculated from the complex potential eq. (1) for temperatures $T = 170$ (solid curves) and 250 MeV (dotted curves) as functions of the gluon energy E_g. The thermal gluon distribution (rhs scale, solid curve for $T = 170$ MeV, dotted for 250 MeV) is used to obtain the thermally averaged gluodissociation cross sections.

F. Brezinski and GW, PLB 707 (2012) 534 / F. Nendzig and GW, Proc. HP12 Cagliari

Thermally averaged gluodissociation cross sections

$$< \sigma_{diss}^{nS} >= \frac{g_d}{2\pi^2 n_g} \int_0^\infty \sigma_{diss}^{nS}(E) \, \frac{p^2 dp}{\exp\left[E(p)/T\right] - 1}$$

Table 1: Thermally averaged cross sections $< \sigma_{diss}(nS) >$ in mb for the gluodissociation of the $\Upsilon(1S), (2S), (3S)$ states at four different temperatures T and $m_g = 0$ in 2.76 TeV PbPb. The values include screening as described in the text; $2S$ and $3S$ states are screened completely at high T.

T (MeV)	$< \sigma_{diss}(1S) >$ (mb)	$< \sigma_{diss}(2S) >$ (mb)	$< \sigma_{diss}(3S) >$ (mb)
400	0.094	–	–
300	0.141	0.041	–
200	0.124	0.465	0.152
170	0.080	0.783	0.604

Gluodissociation width of the Y(nS) states: Cross section x gluon density

Damping and gludissociation width of the Υ(nS) and χ_b(nP) states

- Gludissociation and Collisional (damping) width are of the same order of magnitude
- Damping becomes dominant at T ≥ 300 MeV
- Since the excited states melt due to screening at high T, damping and gludissociation are relevant for these states only at low temperature.

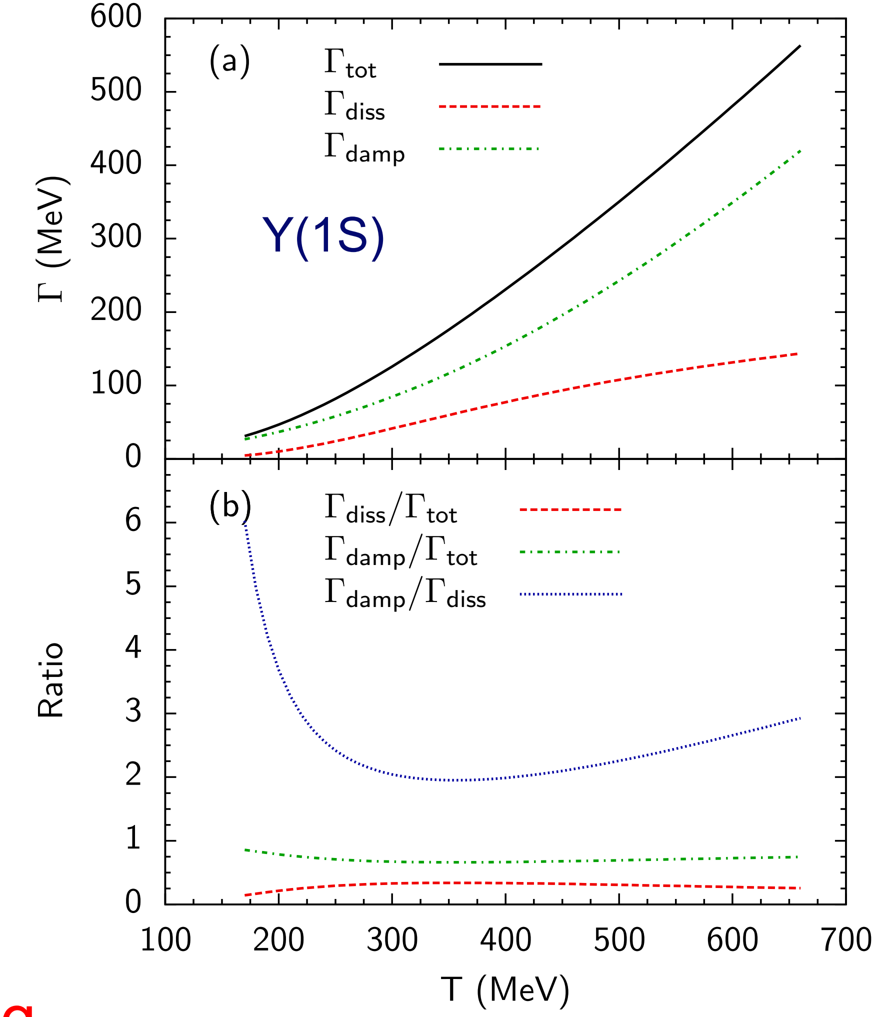

Υ(1S) very stable wrt screening

From: F. Nendzig and G. Wolschin, PRC 87, 024911 (2013)

Dynamical fireball evolution

Dependence of the local temperature T on impact parameter b, time t, and transverse coordinates x, y (Bjorken scaling for the time evolution):

$$T(b,t,x,y) = T_c \, \frac{T_{AA}(b,x,y)}{T_{AA}(0,0,0)} \left(\frac{t_{\rm QGP}}{t}\right)^{1/3}$$

with the nuclear overlap (thickness function) T_{AA} (b,x,y).

The number of produced $b\bar{b}$-pairs is proportional to the number of binary collision, and the nuclear overlap

$$N_{b\bar{b}}(b,x,y) \propto N_{\rm coll}(b,x,y) \propto T_{AA}(b,x,y)$$

Preliminary suppression factor (without feed-down):

$$R_{AA}^{\rm prel} = \frac{\int d^2b \int dx dy \, T_{AA}(b,x,y) \, e^{-\int_{t_F}^{\infty} dt \, \Gamma_{\rm tot}(b,t,x,y)}}{\int d^2b \int dx dy \, T_{AA}(b,x,y)}$$

Feed-down cascade including χ_{1P} and χ_{2P} states

Relative initial populations in pp computed using an inverted cascade from the final populations measured by CMS and CDF(χ_b) [N_{final}(1S):=1]

$N_{initial}$

3S: 0.387

2S: 0.371

1S: 0.458

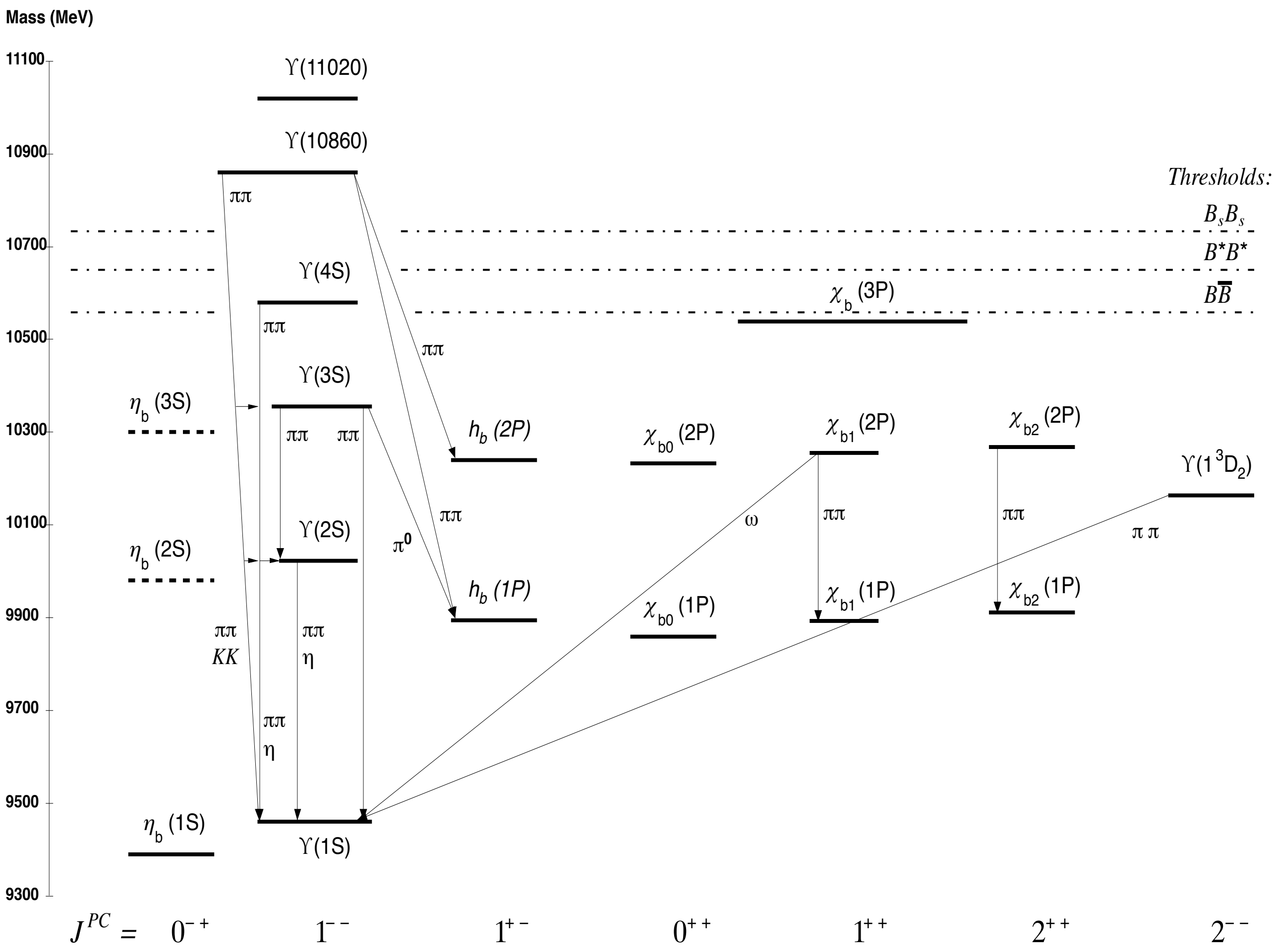

$N_{initial}$

2P: 0.976

1P: 1.29

Theoretical vs. exp. (CMS) Suppression factors

- Screening (potential model)
- Gluodissociation (OPE with string tension included)
- Collisional damping (imaginary part of potential)
- Feed-down from excited states

t_F: Y formation time
t_{QGP}: QGP lifetime
T_{max} @ t_F: 200-800 MeV

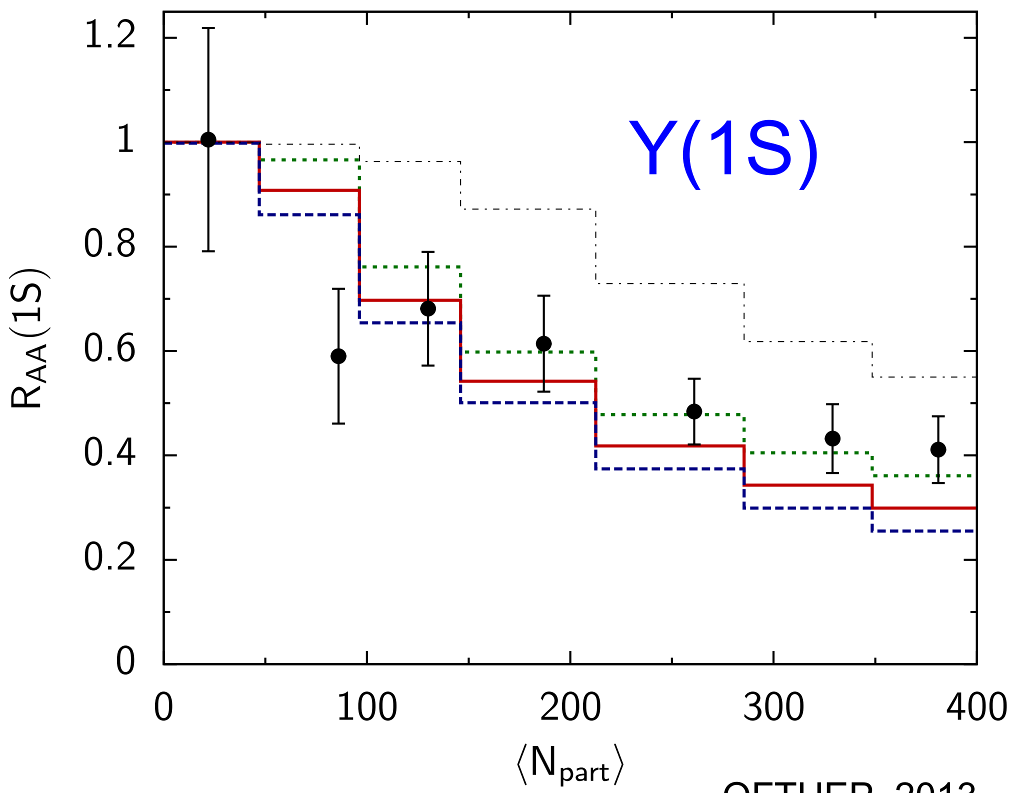

t_F= 0.1 fm/c
t_{QGP}= 4, 6, 8 fm/c

QFTHEP_2013

Theoretical vs. exp. (CMS) Suppression factors

- Screening (potential model)
- Gluodissociation (OPE with string tension included)
- Collisional damping (imaginary part of potential)
- Feed-down from excited states

t_F: Y formation time
t_{QGP}: QGP lifetime
T_{max} @ t_F: 200-800 MeV

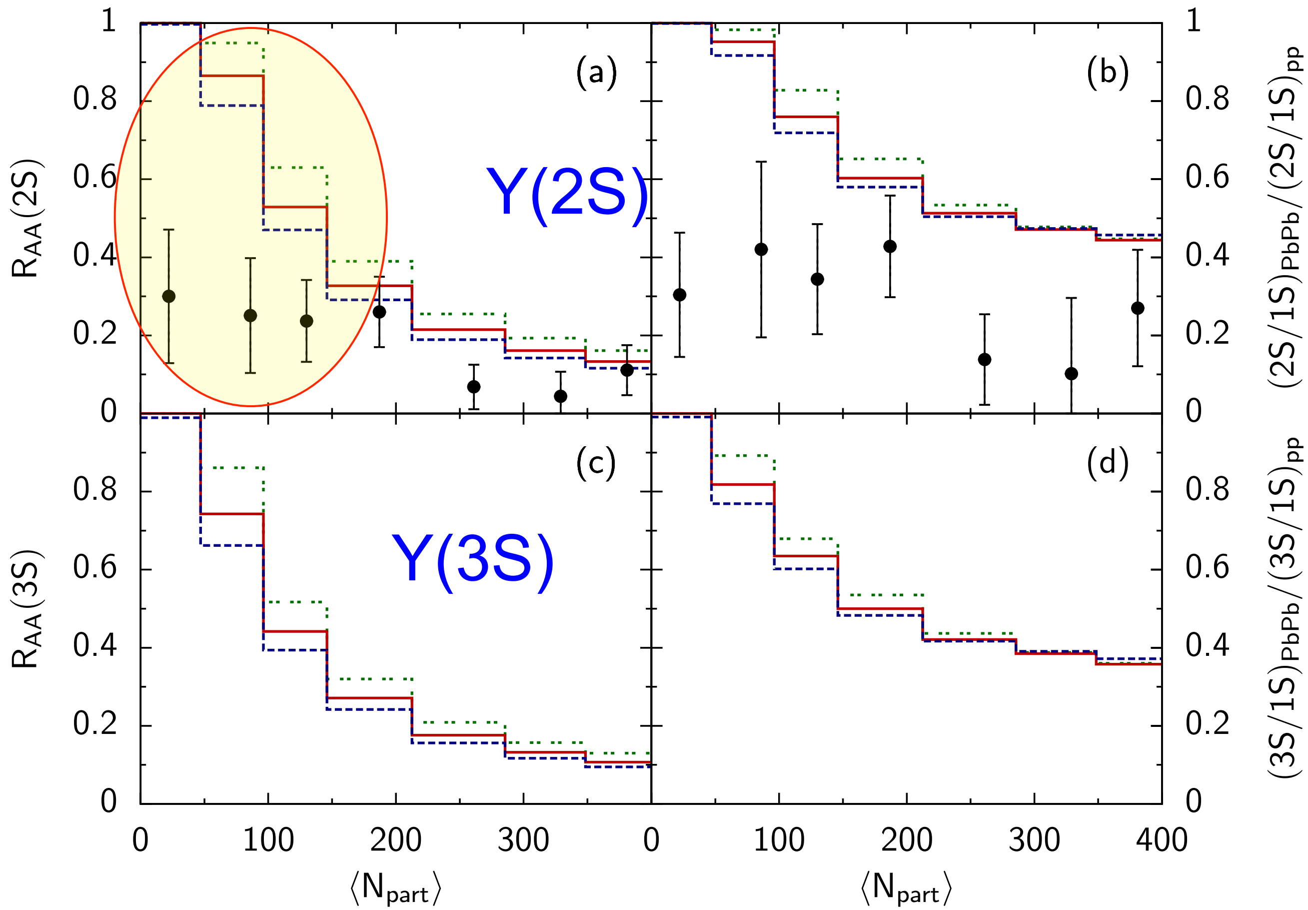

t_F= 0.1 fm/c
t_{QGP}= 4, 6, 8 fm/c

Leaves room for additional suppression mechanisms in particular, for the excited states.

Conclusion 4: Upsilon suppression

- The suppression of the $\Upsilon(1S)$ ground state in PbPb collisions at LHC energies through gluodissociation, damping, reduced feed-down and screening has been calculated for min. bias, and as function of centrality, and is found to be in good agreement with the CMS result. Screening is not decisive for the 1S state except for central collisions.

- The enhanced suppression of the $\Upsilon(2S, 3S)$ relative to the 1S state in PbPb as compared to pp collisions at LHC energies (CMS) is consistent with the model within the (large) error bars for central collisions. There is room for additional suppression mechanisms, in particular for peripheral collisions where discrepancies to the CMS data persist. Screening is very relevant for the excited states.

Thank you for your attention, and for organizing QFTHEP !